ORIGINAL ARTICLE

lajss.org
Latin American Journal of Solids and Structures

www.lajss.org

Assessment of the structural condition of a cable-stayed footbridge based on dynamic tests

Danilo de Santana Nunes[a]*, José Luis Vital de Brito[b], Graciela Nora Doz[c]

[a]Departamento de Engenharias e Computação, Universidade Estadual de Santa Cruz, 45662-900 Ilhéus BA, Brasil. E-mail: dsnunes@uesc.br
[b]Departamento de Engenharia Civil e Ambiental, Universidade de Brasília, 70910-900 Brasília DF, Brasil. E-mail: jlbrito@unb.br
[c]Departamento de Engenharia Civil e Ambiental, Universidade de Brasília, 70910-900 Brasília DF, Brasil. E-mail: graciela@unb.br

* Corresponding author

https://doi.org/10.1590/1679-78257847

Abstract

This paper presents an investigation on the structural condition of a cable-stayed footbridge based on data collected in two dynamic tests, performed at different times. The natural frequencies and mode shapes were obtained by applying output only modal identification methods. At least four experimental mode shapes of the footbridge and stay cables were identified in Operational Modal Analysis. A 3D finite element model of the footbridge was calibrated by adjusting its dynamic properties to the experimentally identified in the first test. The procedure showed, besides an approximation of the dynamic behavior, an approximation of its static behavior, which was confronted to the structural design. The analysis found a discrepancy between the required reinforcement based on the updated model stresses and the existing steel reinforcement. The second test, performed one year later, provided different natural frequency values to those found in the first test and the spectrum presented inconsistency in one of its peaks. It was concluded that the structure presents conditioning problems, thus warning to future structural problems.

Keywords

Structural condition, cable-stayed footbridge, dynamic tests, dynamic behavior, static behavior

Graphical Abstract

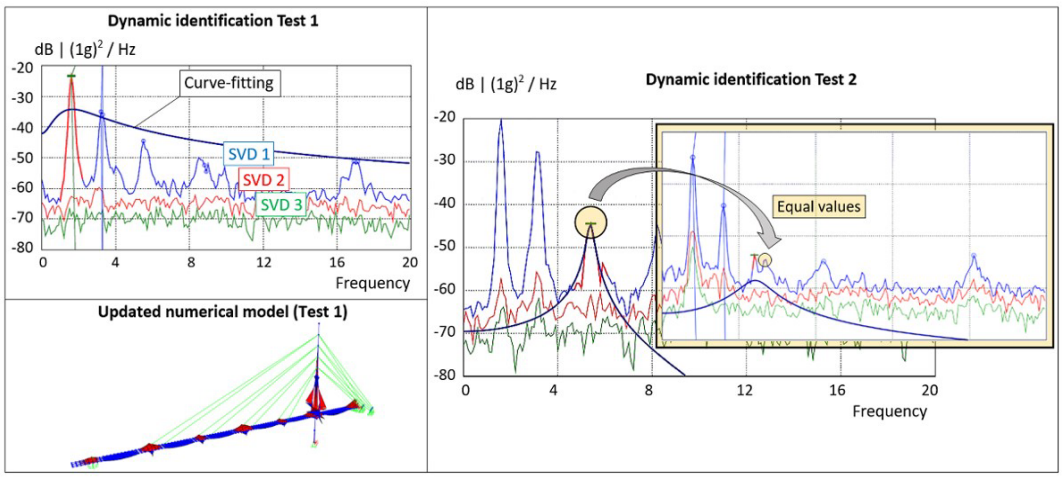

Received: September 26, 2023. In revised form: November 22, 2023. Accepted: December 12, 2023. Available online: January 09, 2024.
https://doi.org/10.1590/1679-78257847

1 INTRODUCTION

Civil engineering structures are subjected to damage resulting from extreme events or accumulated over time due to various sources, under normal use or during overuse and overloading (Nozari et al. 2017; Sanayei et al. 2015), such as environmental, operational, and/or human-induced factors. Consequently, these structures are susceptible to deterioration, degradation, corrosion, fatigue, creep, shrinkage, and erosion, among other problems. Therefore, it is important to monitor structures throughout their useful life and maintain their functioning, thus improving life cycle performance, preventing potential catastrophic events, ensuring safety, and protecting human lives (Abdeljaber et al. 2017; Ren and Peng, 2005; Xu et al. 2012; Dackermann et al. 2014; Dackermann et al. 2018). These analyses generally involve accurate numerical modeling of the structure. These models must be calibrated, usually in terms of the material parameters and boundary conditions, according to on-site responses to dynamic loads (Bayraktar et al. 2009; Chisari et al. 2015). The data obtained via nondestructive tests and the resulting modal parameters estimated through operational modal analysis (OMA) can be used in the structural model updating (MU) and structural health monitoring (SHM) processes. These processes can provide information to the vibration-based assessment of the current and long-term condition of the structure and promote the possible development of alert systems to warn against structural risk (Sanayei et al. 2015; Macdonald and Daniell, 2005; Ubertini et al. 2013; Siringoringo and Fujino, 2008). Structural models that have been verified, refined, and tuned to actual measurements can reduce the uncertainties in SHM, thus providing a good basis for management decisions (Schlune et al. 2009; Cismaşiu et al. 2015; Dall'asta et al. 2016). A continuous SHM is necessary for early identification and localization of any potential damage (Ren and Peng, 2005; Soria et al. 2016). Sun et al. (2020) show that dynamic properties, usually obtained from large volume of experimentally data of the SHM process, are still a useful evaluation tool for assessment of structural condition and non-destructive damage identification in large structures.

This study used a cable-stayed footbridge as a study case. Due to their aesthetic appearance, efficient use of structural materials and other important advantages, cable-stayed structures have gained great popularity in recent decades. There has been a remarkable increase globally in special civil construction projects using this structural solution, whose basic premise is to support the deck with almost-straight cables, known as stay cables or stays. However, these structures may present service problems, raising concerns regarding the structure slenderness and catenary of the cables. Additionally, deferred (concrete shrinkage and creep and steel relaxation) and immediate (cable anchorage and immediate concrete deformation due to the effect of cable pre-tensioning) losses in the components may change the initial equilibrium scheme of the structure and the deformed shape, thus increasing the high stresses and safety problems of the structure under normal use. These aspects reinforce the need for an additional step after design and construction, the structural monitoring.

The Ambient Vibration Test (AVT) was used in this study. Besides the ambient and operational vibration (pedestrians), for the global tests, two people ran and jumped along the footbridge deck while acceleration data were recorded. Three sensors were placed at selected points along the footbridge deck and tower. Four flexural mode shapes were identified in the 0–9 Hz frequency range using two output-only dynamic identification methods. The Curve-fit Frequency Domain Decomposition (CFDD) (Jacobsen and Andersen, 2008; Jacobsen et al. 2008) was used.

The vibration method was also applied to analyze and determine the stay cable forces. The AVT was performed, and the excitation was enhanced by a manual, and randomly, imposed initial displacement. One sensor recorded the acceleration time series, and the Basic Frequency Domain (BFD), commonly called the Peak-Picking method (PP), was used to identify the natural frequencies of the stays.

After performing the experimental tests and identifying the selected dynamic properties (natural frequencies and mode shapes), the numerical model of the footbridge was updated. To analyze the dynamic behavior of cable-stayed structures, finite element models (beam elements, surfaces, and solids) have been used for the tower (Zhang et al. 2001; Yue and Li, 2014) and deck (Park et al. 2012; Park et al. 2015; Zhu et al. 2015; Asadollahi et al. 2018), and the specific model denominated "spine" for the deck (Zhang et al. 2001; Yue and Li, 2014), each with a certain degree of success. Another particularity of cable-stayed structures is the modeling of the stay cables. In the literature, these elements have been simulated as truss elements (Zhang et al. 2001; Yue and Li, 2014; Park et al. 2012; Zhu et al. 2015), by considering the second-order effects caused by their weight through an equivalent modulus of elasticity, and "catenary" elements (cable elements) directly accounting the deformed shapes as function of cable length and force (Park et al. 2015; Asadollahi et al. 2018). The system matrices can be updated via manual and/or automatic tuning, usually based on a preliminary sensitivity check of the updating parameters. Manual tuning is performed directly on the numerical model by the operator. Automatic tuning uses sensitivity-based optimization to construct the final model so that changes to the updating parameters are also minimized by their inclusion in the objective function (Park et al. 2012; PARK et al. 2015; Benedettini and Gentile, 2011; BURSI et al. 2014; Bedon et al. 2016). This study used one-dimensional finite elements to simulate the concrete elements and "catenary" elements for the stays. The model was manually adjusted based on the experimental dynamic properties obtained in the first dynamic test. The procedure was guided by the sensitivity analysis of natural frequencies to changes in selected material properties. The required steel reinforcement, obtained through the stresses of the updated numerical model, was compared to the existing steel reinforcement provided by the structural design.

To establish periodicity in SHM, a new test (Test 2) was performed one year after the first one. The experimental natural frequency values and the Power Spectral Density (PSD) functions of the recorded acceleration signals were compared.

This study focused on investigating the structural condition of a cable-stayed footbridge based on experimental information, through the follow steps: *i*) dynamic testing of the stay cables and complete structure; *ii*) identification of the natural frequencies of the stays using a dynamic identification method, in order to determine the prestressing forces through the Mersenne/Taylor Law for cables pinned at both ends (Gomes, 2006). The cable length was obtained from the solid model, i.e., it was the length between the concrete element faces; *iii*) identification of the dynamic properties (natural frequencies and modes of vibration) of the structure using stochastic modal identification methods, given the difficulty of using deterministic excitations and even interrupting the operation of infrastructure constructions, as is the case with cable-stayed structures (bridges and footbridges); *iv*) design and updating of the numerical model of the structure by inserting the experimental prestressing forces of the stays into the numerical model and optimization of the materials properties and boundary conditions process; *v*) analysis of the current efforts of the structure, provided by the updated numerical model, in comparison with the structural design, so as to identify overloaded regions; *vi*) new testing and updating stages at pre-defined age intervals, using the updated numerical model as a reference, in order to identify any variations in the dynamic properties and stay forces that could characterize a change in the stiffness and equilibrium condition of the structure.

Both Test 1, which identified a divergence between the bending moments' distribution obtained with the updated model and the longitudinal distribution of steel reinforcement provided by the structural design, and Test 2, in which variations in the experimental natural frequency values and in the prestressing forces of the stays were identified, and a discontinuity in the PSD functions was observed, warn about the possibility of future structural problems with the footbridge in service.

2 THE CABLE-STAYED FOOTBRIDGE

2.1 Technical features

The cable-stayed footbridge crosses the BR101 highway at km 88, in the city of Nossa Senhora do Socorro, Sergipe State, Brazil (see Figure 1). The deck is 58.0 m long and 2.0 m wide, divided into two parts by a single central mast 22.4 m tall. The semi-fan cable arrangement of the bridge is distributed spatially in two inclined planes on each side of the deck. Each plane has eight stay cables. Half of the 16 cables are backstays, anchored externally to a foundation block. All of the stays use 32 mm-diameter Dywidag bars, and the superstructure concrete has f_{ck} = 30 MPa (design value). Figure 2 shows the details of the structure. The footbridge presented problems with the foundation system after the construction. The mast rotated in the highway direction due to displacement of the anchorage block and, consequently, the deck deformed shape was modified. The problems were solved, and the footbridge shape was adjusted by applying new forces to the stay cables. This information motivated the investigation.

Figure 1 Cable-stayed footbridge in Sergipe, Brazil.

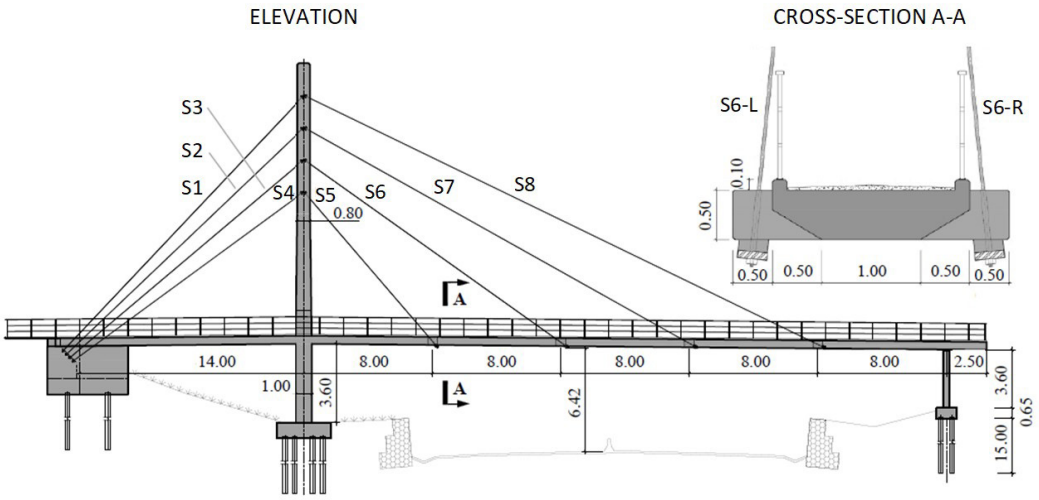

Figure 2 Footbridge details.

2.2 Initial numerical model

A 3D finite element model was created to investigate the footbridge, based on structural design information and field measurements using SAP2000 v24.2.0 software. One-dimensional elements with six-degree-of-freedom at each node were used for the deck and tower, and cable elements with undeformed length were used for the stay cables, totaling 349 finite elements, 16 cable elements, 468 nodes, and 2808 degrees of freedom. The concrete weight per unit volume was assumed to be 25.0 kN/m^3 and the modulus of elasticity to be 30 GPa. The cable (Dywidag bar) weight per unit volume provided by the manufacturer was 76.9415 kN/m^3 and the modulus of elasticity was 205 GPa (± 5%). The boundary conditions between the deck and tower, the deck and anchorage block, and the tower and foundation were considered fixed for rotations and displacements. The pylon support was assumed to be fixed for displacements only, as well as the connection between the stay cables and the anchorage block. The numerical model, used here only to define the test setups through the theoretical mode shapes, presented perfect contact and sliding boundary conditions, which were adjusted based on the experimental results from Test 1. In details, the structural elements were simulated as follows:

i) Deck – four 3D beam elements with equivalent stiffness were used. The cross-section was divided into four parts; the moment of inertia and the centroid showing the longitudinal equivalent element (LE) positions were calculated for each part. 3D beam elements were also used to simulate the transverse stiffness of the deck. The boundary conditions between the deck and tower, and the deck and anchorage block were assumed to be fixed as it is encastre at these connections. The pylon support was assumed to be fixed for displacements only as the connection is via neoprene bearings. Figure 3 illustrates the approach on defining the mesh of the deck.

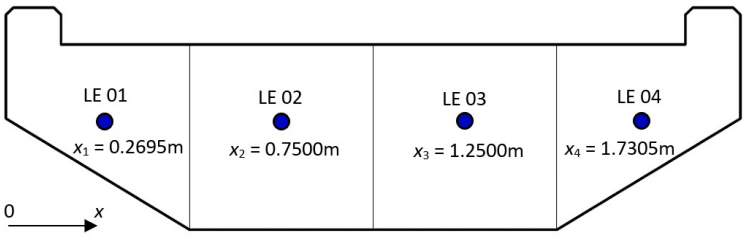

Figure 3 Detail of the division of the deck cross-section to define the stiffness and positions of the longitudinal elements.

To homogenize the distribution of the longitudinal elements, as the difference was very small, the coordinates of the elements LE 1 and LE 4 were modified, respectively, to x_1 = 0.2500 m e x_4 = 1.7500 m. In this way, the transverse distance between all longitudinal elements was 0.50 m. The moments of inertia were calculated in relation to the centroidal axes, without these adjustments. The longitudinal distance between all transverse elements was also adopted of 0.50 m, totaling 336 finite elements for the deck. The stiffness of the one-dimensional transverse elements was calculated for the 0.5 m half-widths between them.

ii) Tower – 3D beam elements considering the structural design cross-section were used; for this, 13 finite elements were needed. The boundary conditions between the tower and foundation were assumed to be fixed as the connection is via deep foundation.

iii) Stay cables – 16 catenary elements were used. They directly consider the nonlinearity caused by the deformed shape of cables due to self-weight. The stay forces measured on-site were added to the model through tools implemented in SAP2000.

Figure 4 shows the initial numerical model, designed with the resulting mesh of the deck, and nine first mode shapes provided by the model and their respective natural frequencies.

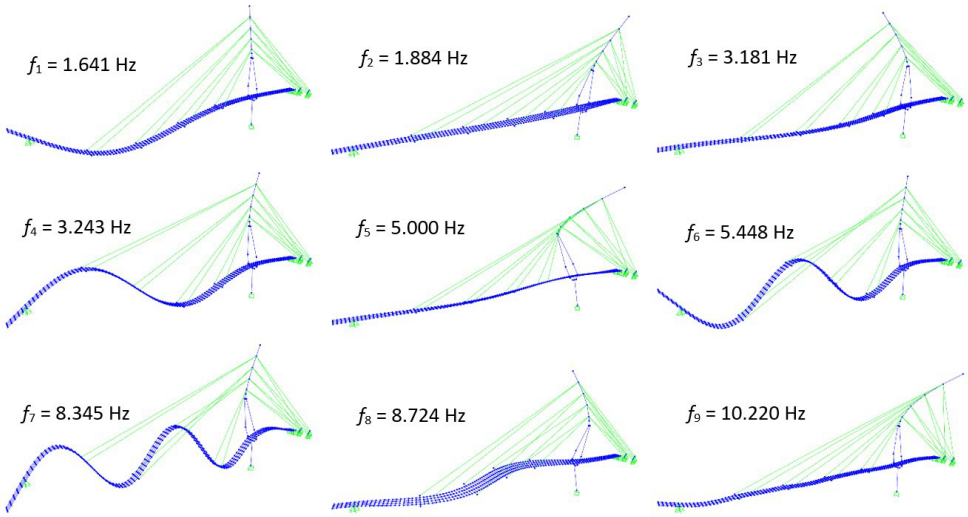

Figure 4 Theoretical mode shapes provided by the initial numerical model.

This study used a simpler approach for designing the numerical model of the cable-stayed footbridge, in contrast to the current trend toward more refined models. It reduced the required computational effort and brought the analysis closer to the structural design approach, which was used as reference for the assessment. The current steel reinforcement was compared to the moment distribution of the updated numerical model. It was important to use a numerical model with similar refinement level to that probably used in structural design.

3 MATERIALS AND METHODS

3.1 Data acquisition system and dynamic tests

Literature reviews on structural monitoring, methods for vibration measurements, and detection of changes in physical parameters or damage detection of structural systems are currently very important. New ideas have recently been proposed for recording the ambient vibration response of structures (Soria et al. 2016; Negulescu et al. 2013; Xu et al. 2019). As an alternative, and due to the impossibility of using professional accelerometers on-site, this study selected the Arduino platform, specifically the Arduino/Genuino 101 board, in combination with RealTerm software to capture and record the acceleration time series. The device is capable of measuring acceleration signals through the Bosch BMI160 Inertial Measurement Unit (IMU). The chip contains a three-axis accelerometer and gyroscope that can be used with a sampling frequency around 200 Hz, which is usually used to extract low-frequency modes such as civil structures, perform recordings in the ±2 g measurement range, with 16384 LSB/g sensitivity and 180 μg/√Hz typical output noise. The board can be supplied with the following specifications: 7–12 V (via DC power jack), 7–12 V (via VIN pin), or 5 V (via USB connector), the latter of which was used in this study. The board was programmed with the Arduino software (IDE), by selecting “Arduino/Genuino 101” in menu “Tools” > “Board”. The software provides the base code to register accelerations. Changes were made in the code to improve the output appearance and sampling frequency. The proposed data acquisition system was previously tested by the research team in different laboratory models. The experiments were compared to professional accelerometers, with promising results. Even though the acquisition system exhibited some noise, it was possible to identify the dynamic properties of the structural models by using the recorded signals. All the details regarding the acquisition system can be found in Nunes (2019).

Two methods were used in the dynamic identification, both in the frequency domain. For the cable tests, to determine just the natural frequencies of the system, the Peak-Picking (PP) Method was applied, thus one sensor was used. For the complete structure tests, where it was also necessary to obtain the mode shapes, the Curve-fit Frequency Domain Decomposition Method (CFDD) and three sensors in 17 setups along the deck and tower were used, with one board as a reference, to calibrate energy content and normalize signals, and two as mobile sensors. The reference sensor position was shown to be promising because significant coordinates were observed for almost all the theoretical mode shapes provided by the initial numerical model of the footbridge, illustrated in the previous section (see Figure 4). The accelerations were recorded in three directions. However, only the z-direction in the deck and y-direction in the tower were used in the system identification process, as the footbridge exhibited no significant vibrations in the other directions and the proposed acquisition system was unable to record the resulting acceleration data. Further, the time series analysis showed nearly constant values during the tests. Specifically, values of zero-g were obtained in the x- and y-directions of the deck and x-direction of the tower, and 1g in the z-direction of the tower. It is noteworthy on-site that in addition to the system limitation regarding the accelerometer sensitivity, generating energy signals in the cited directions was difficult. Despite the apparent need observed in the initial numerical model and the intention to position the mobile sensors along the tower, the measurements were performed at heights of up to 2.0 m. It was due to the lack of necessary safety equipment to access the upper regions of the tower and avoid accidents. Figure 5(a) shows the stay cable and complete structure tests, and Figure 5(b) details the test setups used in the global tests.

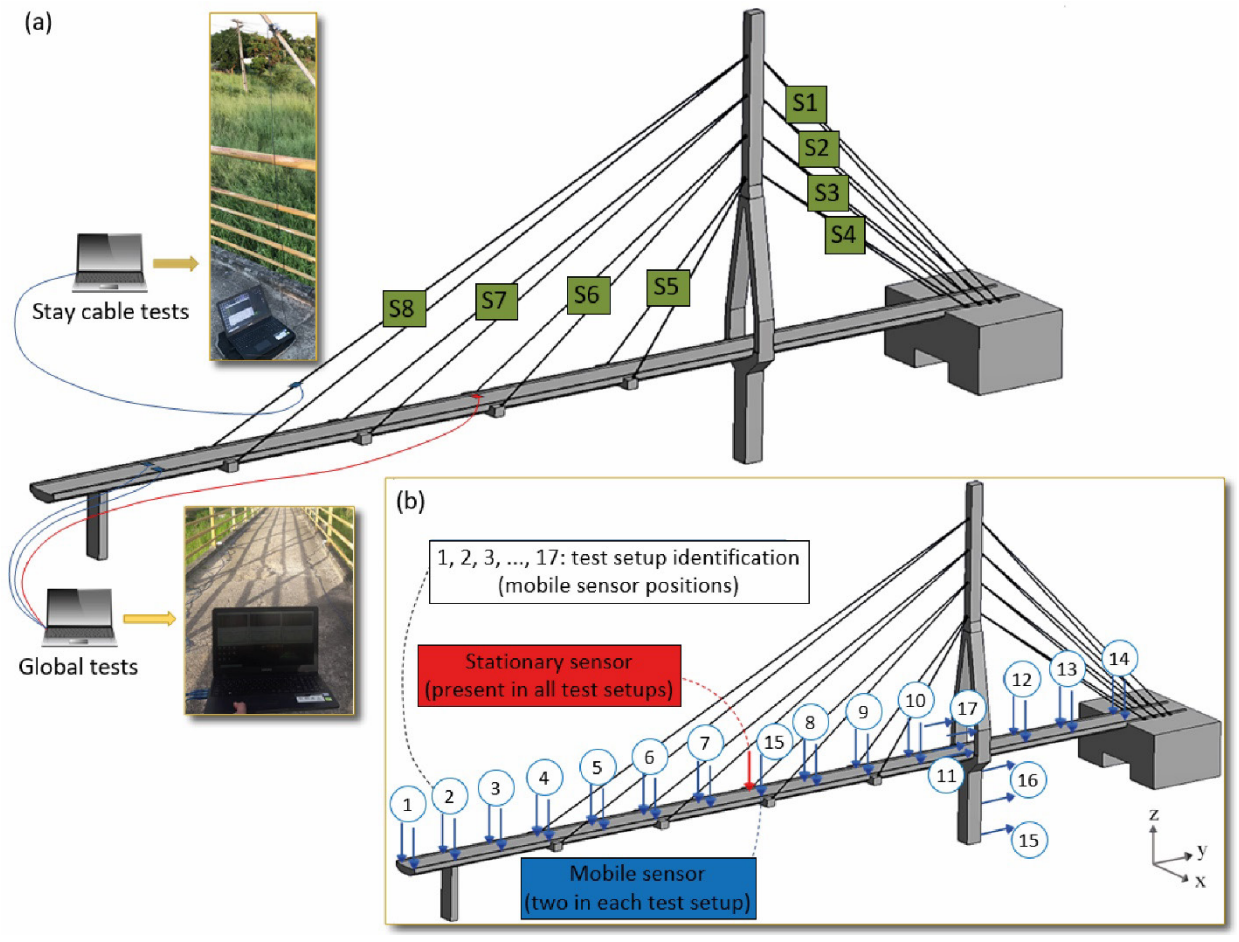

Figure 5 (a) Stay cable and global tests; (b) Test setups used in the global tests.

3.2 Dynamic Structural Identification

3.2.1 Peak-Picking Method (PP)

The PP method uses the Fast Fourier Transform (FFT) to change the time domain into the frequency domain, estimating the Frequency Response Function (FRF) and Power Spectral density (PSD) function of the structure. The DEP function describes how the power of a signal, whether stochastic or deterministic, is distributed along the frequency

values and the natural frequencies of the structure area associated with the peaks of this function. Equation 1 shows how TRF is applied to the correlation functions $R(\tau)$ (auto and crossed), resulting in the DEP function $S(f)$. The correlation functions are used to enable the theoretical calculation of the TRF of stochastic signals, which is the case of the response obtained through environmental vibration tests, since such processes cannot be described with deterministic mathematical expressions.

$$S(f) = \int_{-\infty}^{\infty} R(\tau) e^{-i2\pi f\tau}\, d\tau \tag{1}$$

For multiple degrees of freedom, the spectral information can be organized into matrices using the Equation 2:

$$S_q(f) = H(f)\, S_p(f)\, H^H(f) \tag{2}$$

Where $S_q(f)$ is PSD functions matrix of response, $H(f)$ is FRFs matrix ("^{H}" index means transposed conjugate of matrix), and $S_p(f)$ is PSD functions matrix of excitation.

Mode details about the method can be found in Peeters (2000).

3.2.2 Curve-fit Frequency Domain Decomposition (CFDD)

The CFDD also uses the PSD functions of the response and adopts the following steps:

i) *Calculation of the normalized PSD functions of the response*: Normalization is an artifice used to overcome certain drawbacks when working with several measurement points and test setups, such as the case of infrastructures. This provides a higher number of frequency peaks of each auto-spectrum to be identified, and the variation in excitation intensity during the test, which leads to different energy contents for the measured time series. Thus, it is sought to normalize the energy content of each spectrum, which can be performed by dividing each ordinate of the $PSD_i(\omega)$ function by summation of all ordinates N, resulting in a normalized function $NPSD_i(\omega)$, as follows (Equation 3):

$$NPSD_i(\omega) = \frac{PSD_i(\omega)}{\sum_{k=1}^{N} PSD_i(\omega_k)} \tag{3}$$

ii) Calculation of the average $NPSD_i(\omega)$, the *ANPSD* functions, by Equation 4:

$$ANPSD = \frac{1}{setups} \sum_{i=1}^{setups} NPSD_i\,(\omega) \tag{4}$$

iii) *Singular Value Decomposition (SVD) of the average normalized PSD functions matrix*: The decomposition technique allows decoupling of the spectral density matrix. The matrix is decomposed into spectral density functions of each degree of freedom corresponding to each mode of vibration of the structure;

iv) *Peak selection of the average normalized PSD decomposed in singular values*, which correspond to the structure's natural frequencies;

v) *Weighting of the singular vectors using the respective singular values, and calculation of their average value*: For high singular values, i.e., values closer to the peak, greater weight is given to the respective singular vector in the estimation of the mode shapes. It provides a weighted average estimate of the modes of vibration for each observed degree of freedom and information in the entire region selected for each mode.

vi) *Application of the inverse FFT to the spectral density functions* to obtain the corresponding autocorrelation functions, which are used to estimate the natural frequencies and damping ratios. The adjusted estimates of the natural frequencies can be calculated using linear regression at the instants of passage of the autocorrelation functions through the time axis and at the maximum values, taking into account the relationship between the natural frequency and the damped natural frequency;

vii) *Elimination of the harmonic components using linear interpolation applied to the power spectrum related to the singular value under analysis*, in general the first one;

viii) *Application of the curve fitting algorithm*: The optimization algorithm calculates the function parameters that result in the minimum error, i.e., it determines the curve that best fits the data of the average normalized DEP function decomposed into the first singular value. Furthermore, subsequent use of the algorithm improves accuracy for situations that harmonics are located close to or at the natural frequency value. Linear interpolation, mentioned above, generates

a slight cut in the function peak. It affects the estimation of the natural frequency and overestimates the damping ratio, which can also be circumvented using the algorithm;

ix) *Evaluation of mode shapes through the singular vectors related to the singular values (natural frequencies) obtained at the degrees of freedom* (measurement points).

More details about the method can be found in Jacobsen and Andersen (2008) and Jacobsen et al. (2008).

4 RESULTS AND DISCUSSIONS

The experimental results of this research are presented below. Two stochastic dynamic identification methods were applied. The cable's natural frequencies were identified using the PP method, described above. This technique was implemented using the Matlab software. The cable's natural frequencies were used to estimate the on-site forces of the stays, based on the Vibrating String Mersenne/Taylor Law and considering that the cable is pinned at both ends. The dynamic properties of the system, specifically natural frequencies and mode shapes, were identified from ambient vibration data using the CFDD method. This is available in the ARTeMIS Modal 4.0 software, which was used in this section of the research. The local conditions were similar in both tests. Climatic conditions are quite stable in the city along the year. In addition, the tests were performed exactly one year apart, at the same time of day, and the weather was similar; around 28 degrees, 70% humidity, and no rain. About the excitations, AVT was used but the major excitation was the same in both tests (Test 1 and 2); two people ran and jumped along the footbridge deck to generate enough amplitude for the data acquisition system, and sampling was performed at a frequency of 205 Hz. For the stay cables, AVT was used too, but the major excitations were random displacements, both in direction and magnitude, manually imposed, and the sampling was conducted at a frequency of 210 Hz.

4.1 Dynamic Test 1

4.1.1 Experimental data

Table 1 shows the stay cable axial forces related to the 1st, 2nd, 3rd and 4th natural frequencies obtained from test data and through the PP Method (see Figure 2 to stay cable nomenclature).

Table 1 Stay cable axial forces related to the experimental natural frequencies.

Stay cable	f_1 (Hz)	f_2 (Hz)	f_3 (Hz)	f_4 (Hz)	Average force (kN)	Standard deviation (kN)
S1-R	5.112	10.520	15.440	21.150	275.650	9.038
S1-L	4.979	10.060	15.000	20.780	259.946	10.196
S2-R	4.895	9.956	14.720	20.480	210.161	8.798
S2-L	5.038	10.210	15.180	21.020	222.109	8.549
S3-R	5.064	9.995	15.260	20.790	179.673	5.893
S3-L	5.134	10.100	15.400	21.000	183.608	5.883
S4-R	5.314	11.030	16.410	22.220	165.341	6.344
S4-L	5.094	10.590	15.810	21.410	152.847	6.433
S5-R	5.428	10.960	16.680	22.640	99.145	3.634
S5-L	5.700	11.470	17.430	23.700	108.699	3.750
S6-R	4.420	8.807	13.560	17.850	175.703	4.114
S6-L	4.504	8.976	13.810	18.150	182.211	4.120
S7-R	3.125	6.383	9.376	12.670	178.042	3.716
S7-L	3.128	6.323	9.284	12.550	175.571	3.103
S8-R	2.733	5.465	8.397	11.030	230.710	5.253
S8-L	2.799	5.564	8.530	11.230	239.570	4.422

Figure 6 shows the average normalized PSD function of the signals recorded in the complete structure test, for example, in setup 6 (see Figure 5(b)), decomposed into three singular values (SVD 1, SVD 2 and SVD 3), and the application of the curve-fitting algorithm to the four peaks using the CFDD method.

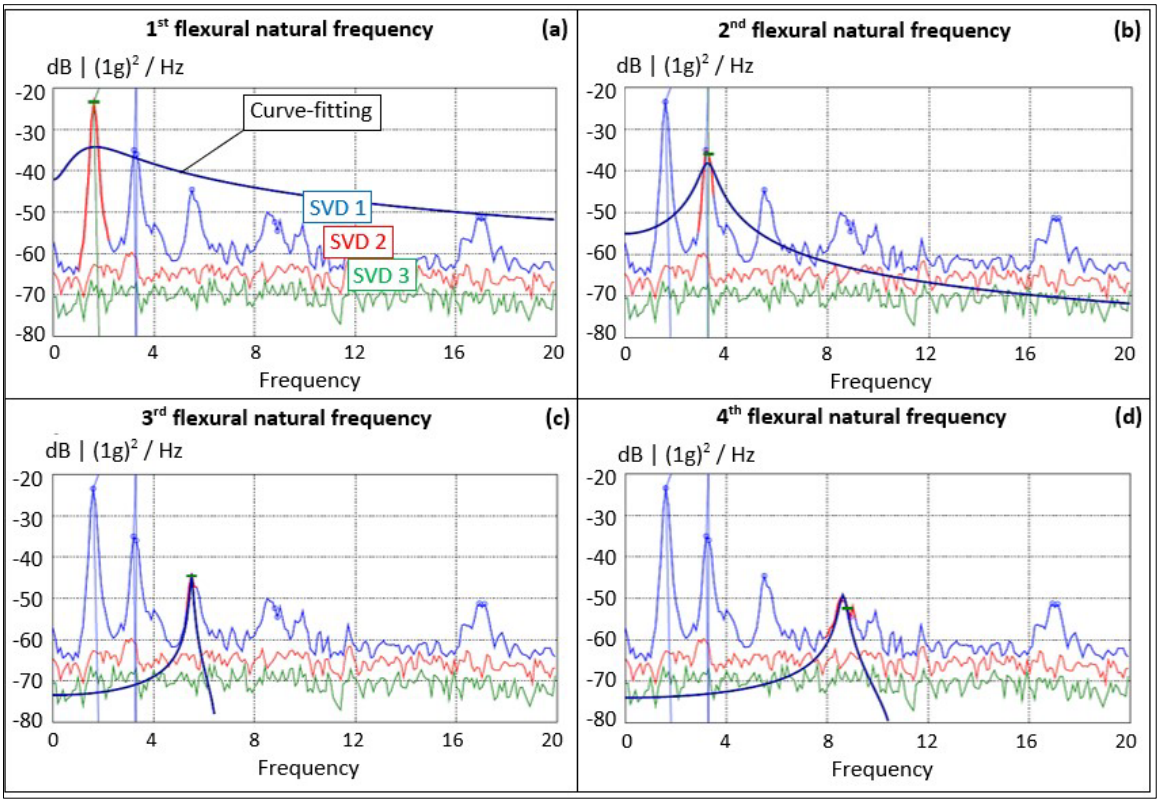

Figure 6 Application of the curve-fitting algorithm to the average normalized PSD functions from Test 1.

4.1.2 Model calibration and equilibrium condition of the structure

The initial model described in section 2.2 has already provided a good correlation between the numerical and experimental dynamic properties (natural frequencies and mode shapes), probably due to the use of undeformed cable elements to model the stays, which leads to forces that simulate deformed shape with zero displacements at the stay-deck connection points. The difference between the frequencies (*DF*) was 1.42% for the first natural frequency and the maximum value of 3.07% was found in the fourth natural frequency (see Table 2). Despite the small differences between the natural frequencies, it was decided to calibrate the numerical model to assess the current efforts of the structure, so as to identify overloaded regions. In addition, numerical models with lower errors provide a better reference in order to identify any variations in dynamic properties, stiffness and equilibrium condition of the structure.

After observing that the first natural frequency was higher in the numerical model compared to the experimental model, altering the boundary conditions of the initial model was the first change made. Translational and rotational springs were inserted considering the properties of the support devices and soil–structure iteration. Based on the dimensions and stiffness of the support device (neoprene) (width, length and height provided by structural design, and transverse Young's modulus provided by manufacturer) and pylon (moment of inertia, height, Young's modulus and boundary condition; assumed fixed-free column), translational springs were calculated to simulate the boundary conditions between the deck and the pylon through the stiffness of the neoprene-pylon-foundation system in deck plane, resulting in longitudinal and transverse springs of 32.5×10^3 kN/m and 6.5×10^3 kN/m, respectively. Rotational springs of 2×10^8 kNm/rad were adopted to simulate the boundary conditions between the tower and the foundation, as well as that between the deck and the anchorage block. The experimental stay forces were inserted in the model. These adjustments resulted in the intermediate model (see Table 2).

This was followed by a sensitivity analysis to evaluate the rate of change of the natural frequencies (from the first to the fourth vertical mode shapes) of the intermediate model due to a +5% change in the selected material parameters. It was used to guide the manual MU process. The Young's modulus of the concrete and concrete weight per unit volume (E_C, and γ_C, respectively), were selected due to all the uncertainties inherent in the use of this material. The Young's modulus of the steel cable (E_S) was selected due to uncertainty according to the manufacturer (± 5% variation around 205 GPa). Figure 7 shows the sensitivity coefficients computed in the analysis.

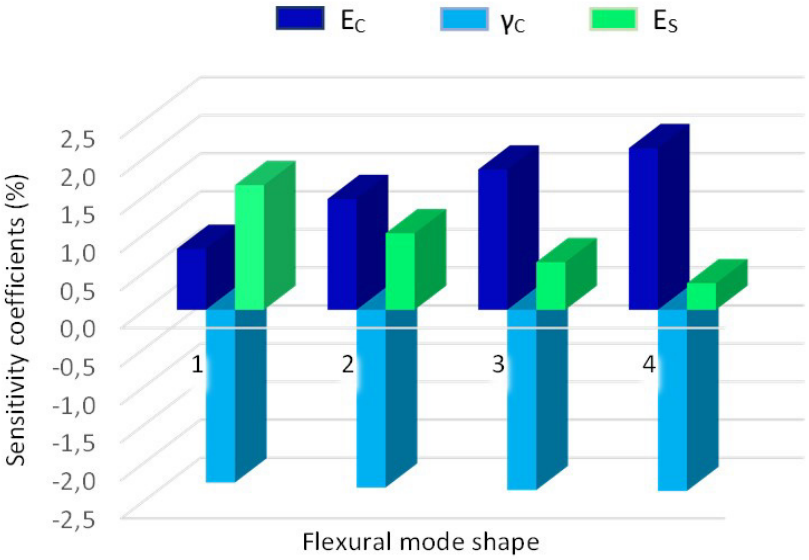

Figure 7 Sensitivity analysis of intermediate numerical model.

The results show that changes in E_C have a greater effect on the higher-order vertical natural frequencies, while changes in E_S have a greater effect on the lower-order vertical natural frequencies. Furthermore, changes in γ_C affect all four first natural frequencies with a similar intensity.

The updating process was performed in three steps. Because the first natural frequency was higher in the intermediate model compared to the experimental model, step 1 consisted of gradually decreasing E_S. Then, because the fourth natural frequency was lower compared to the experimental model, step 2 consisted of increasing E_C. After these steps, the first natural frequency presented a value slightly higher than the experimental value, and thus step 3 consisted of increasing γ_C. Table 2 lists the results obtained from the systematic updating process described above, and Figure 8 shows the updated numerical model.

The approach sought to maximize the index reduction for the first mode shape, which was successfully achieved (FER = 0.00%), combined with a maximum reduction in the difference of the fourth mode shape from 3.07% to 2.52%, resulting in E_C = 31.0 GPa, E_S = 198.5 GPa, and γ_C = 25.3 kN/m^3. The process provided a numerical model with excellent approximation of the system dynamic behavior obtained on-site (the lowest value obtained for the MAC index was 0.937 for the third mode shape), besides an approximation of its static behavior. For assessment of the structural condition, the model was calculated through a geometric nonlinear static analysis, providing the system stiffness to modal analysis. Figure 9 illustrates the bending moments about local x-axis ((a) and (b)) and deformed shape due to self-weight and stay prestressing forces ((c)), experimentally identified. Figure 10 shows the steel reinforcement provided by design. The longitudinal bars positioned at the top of the cross-section, i.e., above the neutral axis, are in red, and the longitudinal bars positioned at the bottom of the cross-section, i.e., below the neutral axis, are in blue.

Table 2 Comparison between the natural frequencies and mode shapes throughout the MU process.

Flexural mode shape	f_{CFDD} (Hz)	Initial Numerical Model E_C = 30.0 GPa, γ_C = 25.0 kN/m^3, E_S = 205 GPa			Intermediate Numerical Model E_C = 30.0 GPa, γ_C = 25.0 kN/m^3, E_S = 205 GPa			→	Updated Numerical Model E_C = 31.0 GPa, γ_C = 25.3 kN/m^3, E_S = 198.5 GPa		
		f_{NM} (Hz)	*DF* (%)		f_{NM} (Hz)	*DF* (%)	Modal Assurance Criterion (MAC)		f_{NM} (Hz)	*DF* (%)	Modal Assurance Criterion (MAC)
1st	1.617	1.640	1.42↑		1.635	1.11↑	0.999		1.617	0.00	0.999
2nd	3.288	3.242	1.40↓		3.242	1.40↓	0.998		3.234	1.64↓	0.998
3rd	5.505	5.447	1.05↓		5.447	1.05↓	0.938		5.460	0.82↓	0.937
4th	8.608	8.344	3.07↓		8.341	3.10↓	0.975		8.391	2.52↓	0.974

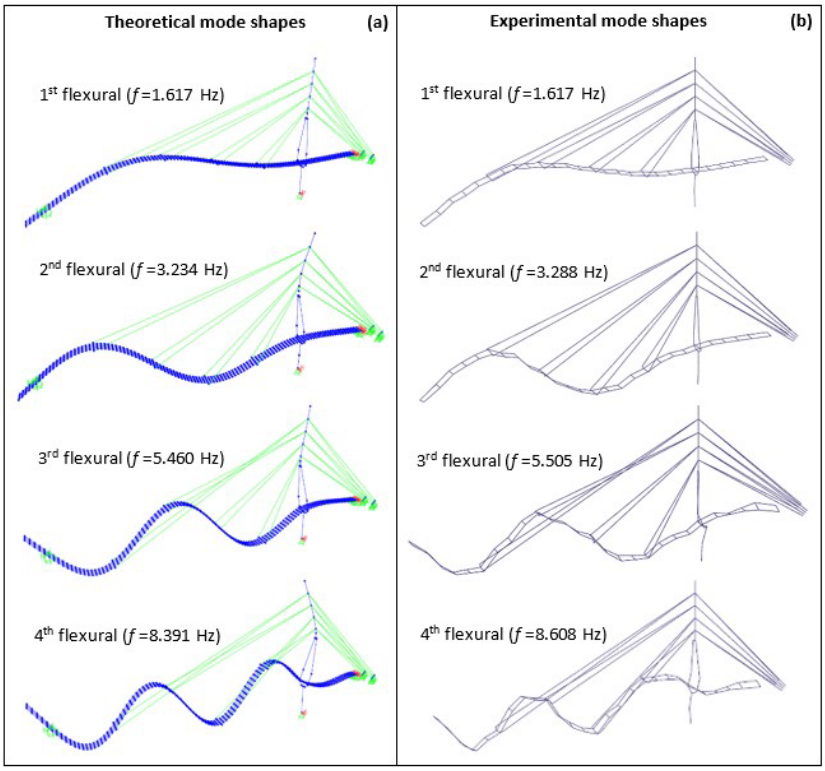

Figure 8 Fist four flexural mode shapes: (a) provided by the updated numerical model; (b) experimentally identified.

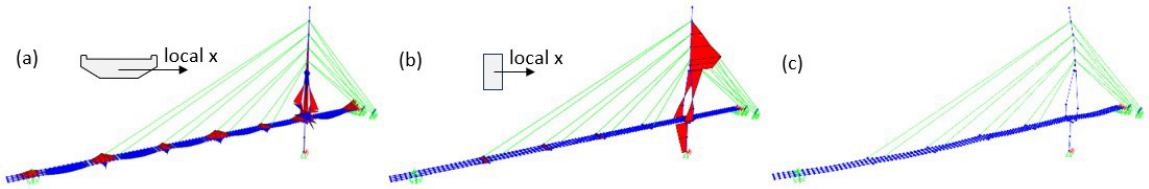

Figure 9 (a) (b) Bending moments about local x-axis (esc.: 1/50) and (c) deformed shape due to self-weight and prestressing forces (esc.: 150/1).

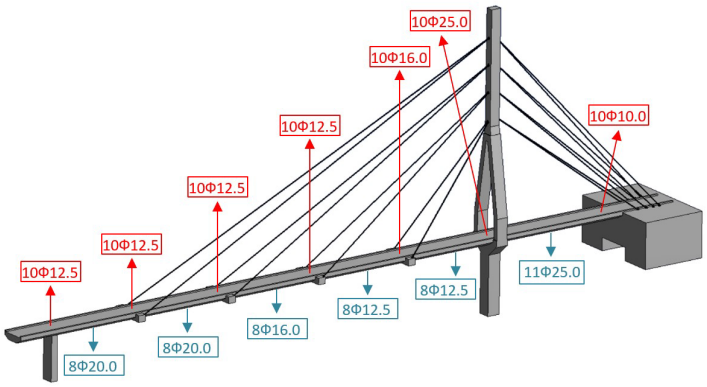

Figure 10 Longitudinal steel reinforcement provided by design.

Stresses that apparently are close to exceed the structural capacity provided by the design and excessive relative curvature of the mast were noticed. The structural design suggests predominance of sagging bending moments greater than hogging bending moments (see Figure 10), different from that provided by the updated numerical model, which presents hogging bending moments at the connection regions between the deck and the stay cables with magnitude greater

than sagging bending moments. The steel reinforcement cross-section was calculated using the bending moments due to self-weight and stay prestressing forces provided by the updated numerical model in the connections between the deck and the stay cable S8, and the stay cable S6. It resulted requested cross-sections, due to self-weight and stay forces, of 9.84 cm^2 (current cross-section: 12.27 cm^2) and 11.11 cm^2 (current cross-section: 12.27cm^2), respectively. It is important to highlight that the bending moments of the updated model were not calculated considering service loads. Various combinations of service loads may occur, which may exceed the structural capacity of the deck at the connections between the stays S8 and S6. Modifications in the structure stresses may occur as a result of changes in the stay prestressing forces, imposed or due to prestressing losses. In fact, as mentioned before, the footbridge had problems in the foundation system. The mast rotated due to displacement of the anchor block and, consequently, the deck presented an unexpected deformed shape. After correcting the position and fixing the anchor block, cable forces were applied in order to adjust the footbridge shape (mast and deck shapes). This event became clear in this research from the analysis of tension stresses and deformed shape of the mast. The new cable forces modified the equilibrium condition of the structure.

4.2 Dynamic Test 2

To assess the structural condition of the footbridge, a new test (Test 2) was done one year after the first one. The Test 1 was performed to update the numerical model. The process was based on the experimental natural frequencies and mode shapes obtained from the acceleration time series recorded in that age. This model served as a starting point (reference numerical model) for investigating any changes in its structural behavior, as well as to management of the footbridge over the years. The second test was similar to the first one in terms of data acquisition system used, excitations and environmental conditions. All stay forces on-site were identified using the same methodology. Table 3 shows the forces obtained in Test 2 and compares them to those obtained in Test 1.

Table 3 Comparative of stay cable forces obtained in both tests.

Stay cable	Dynamic Test 1		Dynamic Test 2		Variation (kN)	Variation (%)	Average variation per pair (%)
	Force (kN)	Standard Deviation (kN)	Force (kN)	Standard Deviation (kN)			
S1-R	275.650	9.038	278.608	9.165	↑ 2.958	↑ 1.07%	0.37 ↑
S1-L	259.946	10.196	259.105	9.713	↓ 0.841	↓ 0.32%	
S2-R	210.161	8.798	214.220	9.520	↑ 4.059	↑ 1.93%	1.04 ↑
S2-L	222.109	8.549	222.456	8.505	↑ 0.347	↑ 0.16%	
S3-R	179.673	5.893	182.563	0.686	↑ 2.890	↑ 1.61%	1.47 ↑
S3-L	183.608	5.883	186.068	5.930	↑ 2.460	↑ 1.34%	
S4-R	165.341	6.344	172.335	6.529	↑ 6.994	↑ 4.23%	8.83 ↓
S4-L	152.847	6.433	119.388	4.677	↓ 33.459	↓ 21.89%	
S5-R	99.145	3.634	102.257	3.533	↑ 3.112	↑ 3.14%	2.73 ↑
S5-L	108.699	3.750	111.222	3.976	↑ 2.523	↑ 2.32%	
S6-R	175.703	4.114	174.007	4.468	↓ 1.696	↓ 0.97%	0.67 ↓
S6-L	182.211	4.120	181.515	4.108	↓ 0.696	↓ 0.38%	
S7-R	178.042	3.716	176.846	3.941	↓ 1.196	↓ 0.67%	0.51 ↓
S7-L	175.571	3.103	174.969	3.166	↓ 0.602	↓ 0.34%	
S8-R	230.710	5.253	233.728	3.541	↑ 3.018	↑ 1.31%	0.89 ↑
S8-L	239.570	4.422	240.688	4.476	↑ 1.118	↑ 0.47%	

The acceleration time series of the stays in both tests (Test 1 and Test 2) were recorded with the same sensor and in the same sequence, from the first to the last stay cable (S1-R to S8-L). The procedure lasted about three consecutive hours in total. Three series were recorded for each stay to verify the consistency of the results, given the impossibility of using professional accelerometers. The experimental natural frequencies provided by the three series of all stays were practically equal.

The Test 2 was reduced to the two setups that presented the highest energy content in Test 1, used to identify the natural frequencies (setup 3 and setup 6), in order to verify any change of the natural frequencies and PSD functions of the structure. Figure 11 shows the average normalized PSD functions of the recorded signals, decomposed into three singular values, and the application of the curve-fitting algorithm to the peaks using the CFDD method. The acceleration time series were obtained in the same test setup (setup 6) used in the dynamic identification of Test 1.

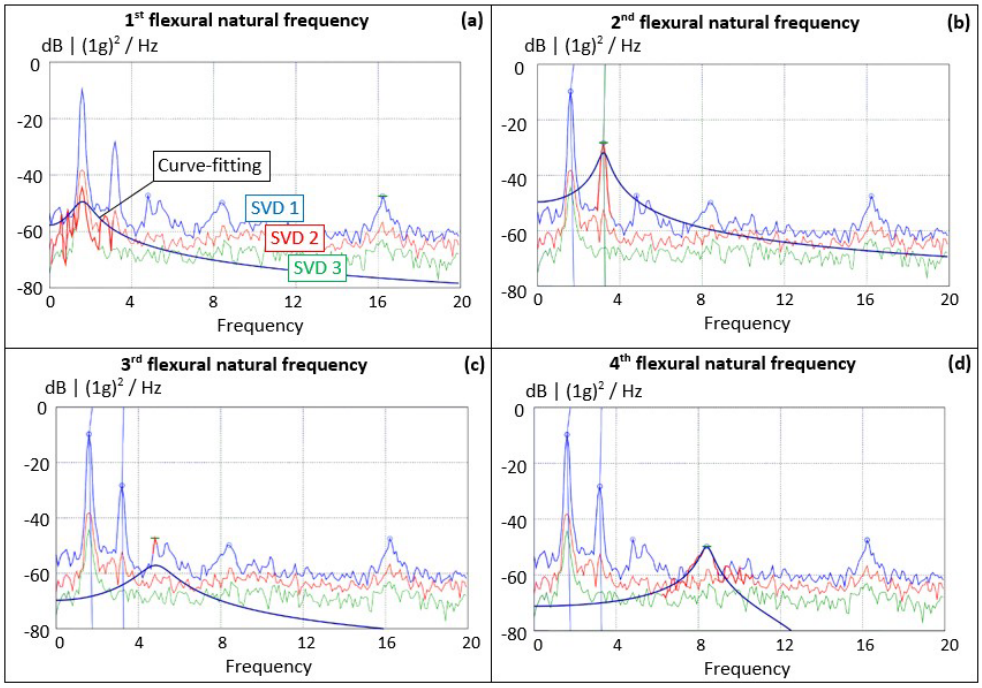

Figure 11 Application of the curve-fitting algorithm to the PSD function using the CFDD method, in setup 6 of Test 2.

The spectrum presented an inconsistency. It provided two very close frequency peaks that difficulted to identify the third flexural natural frequency. This fact did not occur in the first test, a year earlier. The test setup 3, which presented the second-highest energy content, was then used to identify this frequency value. The other frequencies were normally identified using test setup 6. Figure 12 shows the average normalized PSD function of the signal recorded in setup 3, decomposed into three singular values, and applied the curve-fitting algorithm to the third peak. In this case, the third frequency peak presented a well-defined value and equal to one of the two peaks provided by the previous test setup.

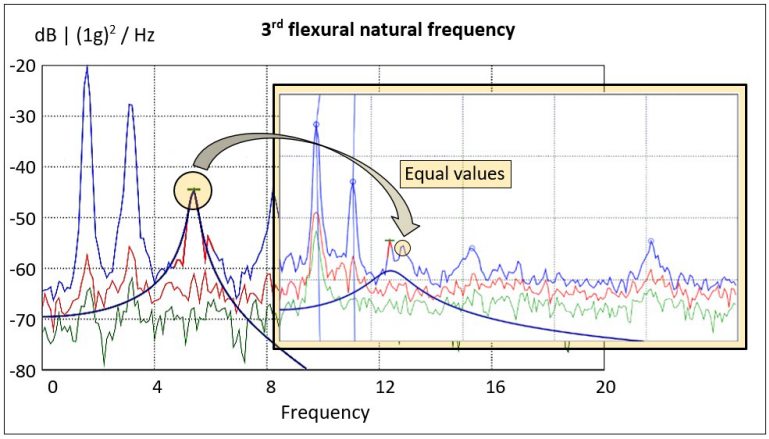

Figure 12 Curve-fitting algorithm applied to the PSD function of the Test 2 using test setup 3 (comparison between both third peaks).

Table 4 lists the modal participating mass ratios of the ten first mode shapes provided by the numerical model. The experimental identified modes are highlighted in bold.

The numerical modes 1, 4, 6 and 8 represent the flexural mode shapes 1, 2, 3 and 4 identified experimentally, which presented modal participating factors of 37.3%, 2.9%, 4.6% and 0.2%, respectively. It was observed that the first three experimental mode shapes contribute more to the final response of the structure among the first ten numerical modes, with emphasis on modes 1 (37.3%) and 3 (4.6%). In other words, these mode shapes have a significant influence on the structural response and on detection of structural anomalies. In fact, as shown previously in Figure 12, the third flexural mode shape presented an inconsistency on spectrum provided by one of the test setups, alerting about a possible structural problem. Table 5 lists and compares the natural frequencies related to the first four flexural mode shapes identified in both tests using the CFDD.

Table 4 Modal participating mass ratios.

Mode shape	Frequency (Hz)	UX	UY	UZ
1st	**1.617**	**2.291E-09**	**0.00110**	**0.37257**
2nd	1.766	0.53804	9.588E-12	2.043E-09
3rd	2.573	0.13446	5.517E-12	1.200E-10
4th	**3.234**	**9.214E-12**	**0.00121**	**0.02924**
5th	4.864	0.03340	1.113E-11	2.022E-11
6th	**5.460**	**2.441E-12**	**0.00250**	**0.04631**
7th	7.287	0.01313	1.884E-13	9.231E-15
8th	**8.391**	**6.618E-15**	**0.00767**	**0.00165**
9th	10.002	1.066E-10	0.09400	0.00510
10th	11.121	0.12374	7.29E-09	1.586E-09

Table 5 Comparison between the first four natural frequencies identified in both tests.

Flexural mode shape (experimental)	$f_{Test\ 1}$ (Hz)	$f_{Test\ 2}$ (Hz)	Difference (Hz)	Difference (%)
1st	1.617	1.616	0.001 ↓	0.06 ↓
2nd	3.288	3.284	0.004 ↓	0.12 ↓
3rd	5.505	5.405	0.100 ↓	1.85 ↓
4th	8.608	8.408	0.200 ↓	2.38 ↓

Reductions in the identified natural frequencies were observed (maximum of 2.33%), which is usually related to stiffness loss of the system. In fact, the greatest force variation suffered by the stays occurred in cable with prestress loss (S4-L with 21.89% loss), indicating stiffness loss of the structural elements affected by this cable. In addition, a relationship between the regions affected by greater redistribution of stay forces and the higher theoretical coordinates, provided by the updated numerical model, of the mode shapes that suffered significant reductions in their natural frequency values (third and fourth flexural mode shapes) was observed. Figure 13 highlights stay pairs that lost prestressing force in red and the stay pairs that suffered an increase in their forces in yellow. Table 6 shows the normalized vertical modal coordinates of the updated numerical model of P1, P2 and P3 points (connection points between the deck and S7, S6 and S5 stays, respectively) illustrated in Figure 13.

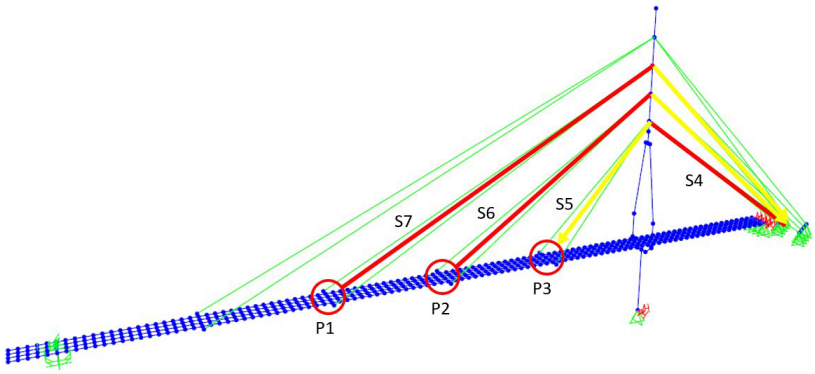

Figure 13 Force variation of the S4, S5, S6 and S7 stays.

Table 6 Normalized modal coordinates (vertical component) of P1, P2 and P3.

Flexural mode shape	Deck point		
	P1	P2	P3
1st	**0.967**	0.563	0.163
2nd	0.049	**1.000**	0.584
3rd	**0.895**	0.075	**1.000**
4th	0.714	**1.000**	**0.989**

The P3 point, located at the connection between S5 stay cable pair and the deck, presents high coordinate values in the third and fourth flexural mode shapes. P3 is directly affected by the S5 stay force, which in turn is directly influenced by S4 stay. S4 stay cable pair presented the greatest force decrease (8.83% loss) between all stay pairs. It is important to point out that the S5 stay pair, which has a force action line that intersects S4 stay force action line at the mast, suffered the greatest force increase (2.73% gain) (see Table 3).

In addition, the results showed relationships between the identification process in Test 2 carried out using test setup 6 (see Figure 5(b)), which was used in Test 1, and the amplitude of oscillations at the mobile sensors points, and the region of the deck located between the stays. The two mobile sensors in setup 6 were located at P1 point of the deck (see Figure 13). The magnitude of oscillations in third mode shape (see Table 6) may have resulted in an undefined frequency at the third spectrum peak, probably due to some structural problem. In order point of view, P1 point is within the region directly affected by the stay cables, which suffered a significant redistribution of forces. The identification problem of the third natural frequency in Test 2 was circumvented using a different test setup from that used in Test 1, specifically test setup 3. This setup used mobile sensors outside the cable-stayed region, specifically between the S8 stay and the pylon (in half way) (see Figure 5(b)).

For verification purposes, the stay forces from Test 2 were applied to the numerical model updated from Test 1 data. This procedure provided the dynamic behavior of the footbridge taking into account the new forces obtained on-site, i.e., verified whether the variations in the natural frequencies of the footbridge between the two tests resulted from variations in the stay forces or from any change in the stiffness of the concrete elements. The four frequencies related to the first four flexural mode shapes were the same as those provided by the numerical model updated in Test 1 when using three significant figures; maximum differences of 0.0001Hz were obtained. In this case, it was observed that the variations in the footbridge natural frequencies, although small, resulted of variations in the stiffness of the concrete elements and/or their connections.

5 CONCLUSIONS

An investigation on the structural condition of a cable-stayed footbridge based on dynamic properties and equilibrium condition of the system was discussed. The procedure began with the structural identification of the footbridge using experimental acceleration time series (Test 1), followed by updating of the numerical model. A new test (Test 2), one year after Test 1, was carried out to identify any variations in the dynamic properties of the footbridge, which would configure a change in equilibrium condition of the structure. It has been confirmed that updated numerical models and periodic test routines are powerful and important tools for managing civil structures, especially for flexible structures, such as cable-stayed structures. In addition, the evaluation of a real structure, with real problems, could be done using recent and affordable numerical tools and measurement devices.

About the case study, it was concluded that the footbridge may present structural problems in the future. Some information from both tests was used on the assessment. The structure shape reconditioning performed by adjusting the stay cable forces (a fact that occurred after construction) was verified through hogging bending moments at the connection regions between the deck and the stay cables with magnitude greater than sagging bending moments provided by the numerical model, different from that provided by the structural design, which suggests predominance of sagging bending moments greater than hogging bending moments. Stresses that apparently are close to exceed the current structural capacity, specifically in the connections between the deck and the stay cable S8, and the stay cable S6; and excessive relative curvature of the mast were noticed by using Test 1 data.

It was difficult to identify, in Test 2, the third natural frequency due to an inconsistency on spectrum provided by one of the test setups. The related mode shape presents significant modal coordinates in the regions affected, directly or indirectly, by loss of prestressing forces. This problem was circumvented using another test setup, which has mobile sensors outside this region. In addition, it is important to emphasize that the third flexural mode shape has the second higher value of modal participating factor (4.6%) among the first ten mode shapes of the footbridge, contributing with some importance to the final response of the structure and on detection of structural anomalies.

Two natural frequency values decreased between the tests. The third flexural natural frequency decreased 1.85% and the fourth natural frequency decreased 2.38%. It was noticed that the mode shapes whose presented significant reductions in their frequencies (third and fourth, among the experimentally identified mode shapes) were those with significant modal coordinates of P3 point. This point is directly influenced by the stays that showed the greatest variations in their prestressing forces (8.83% reduction in S4 stay and 2.73% increase in S5 stay). The modal coordinates of P3 in the first and second mode shapes are close to zero, and their respective natural frequencies just suffered a reduction of 0.06% and 0.12%, respectively. All these aspects support the technical evaluation of this research, which recommends periodic field inspections of the footbridge to define, if necessary, structural reinforcement of the concrete structural elements and/or reconditioning of the stay cable forces.

Author's Contribuitions: Conceptualization, methodology, data analysis, writing - original draft, review & editing, D de S Nunes; Data analysis, writing - review & editing, JLV de Brito; Data analysis, writing - review & editing, GN Doz.

Editor: Marco L. Bittencourt

References

Abdeljaber, O., Avci, O., Kiranyaz, S., Gabbouj, M., Inman, D.J. (2017). Real-time vibration-based structural damage detection using one-dimensional convolutional neural networks. Journal of Sound and Vibration, 388: 154-170.

Asadollahi, P., Huang, Y., Li, J. (2018). Bayesian Finite Element Model Updating and Assessment of Cable-Stayed Bridges using Wireless Sensor Data. Sensors, 18(9): 1-22.

Bayraktar, A., Altunişik, A.C., Sevim, B., Türker, T. (2009). Modal Testing, Finite-Element Model Updating, and Dynamic Analysis of an Arch Type Steel Footbridge. Journal of Performance of Constructed Facilities, 23(2): 81-89.

Bedon, C., Dilena, M., Morassi, A. (2016). Ambient Vibration Testing and Structural Identification of a Cable-Stayed Bridge. Meccanica, 51(11): 2777-2796.

Benedettini, F. and Gentile, C. (2011). Operational Modal Testing and FE Model Tuning of a Cable-Stayed Bridge. Engineering Structures, v. 33: 2063-2073.

Bursi, O.S., Kumar, A., Abbiati, G., Ceravolo, R. (2014). Identification, Model Updating and Validation of a Steel Twin Deck Curved Cable-Stayed Footbridge. Computer-Aided Civil and Infrastructure Engineering, 29(9): 703-722.

Chisari, C., Bedon, C., Amadio, C. (2015). Dynamic and Static Identification of Base-Isolated Bridges using Genetic Algorithms. Engineering Structures, 102(1): 80-92.

Cismaşiu, C., Narciso, A.C., Santos, F.P.A. (2015). Experimental Dynamic Characterization and Finite-Element Updating of a Footbridge Structure. Journal of Performance of Constructed Facilities, 29(4): 1-29.

Dackermann, U., Smith, W.A., Randall, R.B. (2014). Damage identification based on response-only measurements using cepstrum analysis and artificial neural networks. Structural Health Monitoring, 13(4): 430-444.

Dackermann, U., Smith, W.A., Alamdari, M.M., Li, J., Randall, R.B. (2018). Cepstrum-based damage identification in structures with progressive damage. Structural Health Monitoring, 18(1): 87-102.

Dall'Asta, A., Ragni, L., Zona, A., Nardini, L., Salvatore, W. (2016). Design and Experimental Analysis of an Externally Prestressed Steel and Concrete Footbridge Equipped with Vibration Mitigation Devices. Journal of Bridge Engineering, 21(8) C5015001: 1-12.

Gomes, L.M.L.C. (2006). Excitação paramétrica em tirantes de pontes. Master's Thesis (in Portuguese), University of Porto, Portugal.

Jacobsen, N.-J., Andersen, P., Brincker, R. (2008). Applications of Frequency Domain Curve-fitting in the EFDD Technique. In: 26th Conference and Exposition on Structural Dynamics (IMAC XXVI). Orlando. FL: Society for Experimental Mechanics, 1: 518-530.

Jacobsen, N.-J. and Andersen, P. (2008). Curve-fitted Enhanced Frequency Domain Decomposition – A Robust Technique to Harmonic Excitation in Operational Modal Analysis. In: 15th International Congress on Sound and Vibration (ICSV 15). Daejeon. Korea: International Institute of Acoustics and Vibration, 1: 2542-2549.

Macdonald, J.H.G. and Daniell, W.E. (2005). Variation of Modal Parameters of a Cable-Stayed Bridge Identified from Ambient Vibration Measurements and FE Modelling. Engineering Structures, 27(13): 1916-1930.

Negulescu, C., Luzi, G., Crosetto, M., Raucoules, D., Roullè, A., Monfort, D., Pujades, L., Colas, B., Dewez T. (2013). Comparison of Seismometer and Radar Measurements for the Modal Identification of Civil Engineering Structures. Engineering Structures, 51: 10-22.

Nozari, A., Behmanesh, I., Yousefianmoghadam, S., Moaveni, B., Stavridis, A. (2017). Effects of Variability in Ambient Vibration Data on Model Updating and Damage Identification of a 10-Story Building. Engineering Structures, 151: 540-553.

Nunes, D. de S. (2019). Identificação de Sistemas e Detecção de Danos de Estruturas Estaiadas. Ph.D. Thesis (in Portuguese), University of Brasilia, Brazil.

Park, W., Park, J.Y., KIM, H.-K. (2015). Candidate Model Construction of a Cable-Stayed Bridge using Parameterised Sensitivity-based Finite Element Model Updating. Structure and Infrastructure Engineering, 11(9): 1163-1177.

Park, W., Kim, H.-K., Jongchil, P. (2012). Finite Element Model Updating for a Cable-Stayed Bridge using Manual Tuning and Sensitivity-based Optimization. Structural Engineering International, 22(1): 14-19.

Peeters, B. (2000). System Identification and Damage Detection in Civil Engineering. Ph.D. Thesis (in English), Catholic University of Leuven, Belgium.

Ren, W.-X. and Peng, X.-L. (2005). Baseline Finite Element Modeling of a Large Span Cable-Stayed Bridge through Field Ambient Vibration Tests. Computers and Structures, 83(8-9): 536-550.

Sanayei, M., Khaloo, A., Gul, M., Catbas, F.N. (2015). Automated Finite Element Model Updating of a Scale Bridge Model using Measured Static and Modal Test Data. Engineering Structures, 102(1): 66-79.

Schlune, H., Plos, M., Gylltoft, K. (2009). Improved Bridge Evaluation through Finite Element Model Updating using Static and Dynamic Measurements. Engineering Structures, 31: 1477-1485.

Siringoringo, D.M. and Fujino, Y. (2008). System Identification of Suspension Bridge from Ambient Vibration Response. Engineering Structures, 30(2): 462-477.

Soria, J.M., Díaz, I.M., García-Palacios, J.H., Ibán, N. (2016). Vibration Monitoring of a Steel-Plated Stress-Ribbon Footbridge: Uncertainties in the Modal Estimation. Journal of Bridge Engineering, 21(8) C5015002: 1-13.

Sun, L., Shang, Z., Xia, Y., Bhowmick, S., Nagarajaiah, S. (2020). Review of Bridge Structural Health Monitoring Aided by Big Data and Artificial Intelligence: From Condition Assessment to Damage Detection. Journal of Structural Engineering, 146(5) 04020073: 1-22.

Ubertini, F., Gentile, C., Materazzi, A.L. (2013). Automated Modal Identification in Operational Conditions and its Application to Bridges. Engineering Structures, 46: 264-278.

Xu, Y., Brownjohn, J.M.W., Huseynov, F. (2019). Accurate Deformation Monitoring on Bridge Structures Using a Cost-Effective Sensing System Combined with a Camera and Accelerometers: Case Study. Journal of Bridge Engineering, 24(1) 05018014: 1-14.

Xu, B., Song, G., Masri, S.F. (2012). Damage detection for a frame structure model using vibration displacement measurement. Structural Health Monitoring, 11(3): 281-292.

Yue, L. and Li, S. (2014). The Finite Element Model Updating of Long Span Cable-Stayed Bridge based on Static and Dynamic Loading Test. Applied Mechanics and Materials, 644-650: 5014–5018.

Zhang, Q.W., Chang, T.Y.P., Chang, C.C. (2001). Finite-Element Model Updating for the Kap Shui Mun Cable-Stayed Bridge. Journal of Bridge Engineering, 6(4): 285-293.

Zhu, Q., Xu, Y.L., Xiao, X. (2015). Multiscale Modeling and Model Updating of a Cable-Stayed Bridge. I: Modeling and influence line analysis. Journal of Bridge Engineering, 20(10): 1-10.